Hall Dynamics of the Kelvin-Helmholtz Instability

J. D. Huba

Beam Physics Branch, Plasma Physics Division, Naval Research Laboratory, Washington, D.C. 20375

(Received 25 October 1993)

The nonlinear evolution of the Kelvin-Helmholtz instability in an inhomogeneous plasma is studied using a two-dimensional magnetohydrodynamic (MHD) simulation code which includes the Hall term. This term is important when the thickness of the boundary layer is less than an ion inertial length. In comparison to the evolution of the instability based upon ideal MHD, the Hall term generates short wavelength turbulence which inhibits vortex formation, and introduces an asymmetry into the nonlinear evolution of the instability depending upon the sign of the vorticity.

PACS numbers: 52.35.Py, 52.65.+z, 96.35.Kx

The Kelvin-Helmholtz instability has received considerable attention as a mechanism to provide viscous coupling and transport across boundary layers in space and laboratory plasmas. Observational evidence indicates that these boundary layers can be quite narrow, with $L < c/\omega_{pi}$ where L is the thickness of the boundary layer and c/ω_{pi} is the ion inertial length radius [1-5]. Most theoretical work on the subject of thin boundary layers has used kinetic (Vlasov) theory [6], while numerical studies have used hybrid [7-9] or particle [10] codes because standard magnetohydrodynamic (MHD) theory of the instability [11,12] breaks down. However, the validity of MHD theory can be extended to the regime $L < c/\omega_{pi}$ by including the Hall term [13]. Recently, linear theories of the Kelvin-Helmholtz instability have been developed based upon Hall MHD theory [14,15]. One interesting feature of this work is that the Hall term introduces an asymmetry: the linear growth rate is a function of the sign of the vorticity. In addition, Opp and Hassam [14] find a new branch of the instability in the short wavelength regime ($kL > 1$). In this Letter, the first 2D Hall MHD simulation results in the nonlinear evolution of the Kelvin-Helmholtz instability are presented.

The 2D Hall MHD equations used in the analysis are [13]

$$\frac{\partial n_i}{\partial t} + \nabla \cdot n_i \mathbf{V}_i = 0 , \tag{1}$$

$$n_i m_i \frac{d\mathbf{V}_i}{dt} = -\nabla \left(\frac{B^2}{8\pi} + P \right) , \tag{2}$$

$$\frac{\partial \mathbf{B}}{\partial t} + \nabla \times (\mathbf{V}_i \times \mathbf{B}) - \nabla \times \frac{\mathbf{J} \times \mathbf{B}}{n_e e} , \tag{3}$$

where $P = nT$, $T = T_e + T_i$, and $\mathbf{B} = B(x,y)\hat{\mathbf{e}}_z$. The second term on the right-hand side of (3) is the Hall term. Equations (1)-(3), coupled with an equation of state, form a complete set of one-fluid equations describing the ion density and velocity, and the magnetic field. An isothermal equation of state (i.e., $P = nT$) is considered, and $T_e \gg T_i$ is assumed so that finite ion Larmor radius effects can be neglected.

Linear analysis of (1)-(3) yields a dispersion relation [16]

$$\omega = \frac{k_x V_A}{2} \left(\frac{c}{\omega_{pi} L_n} \right) \times \left[1 \pm \left\{ 1 + 4(1+\beta/2) \left(\frac{L_n^2 \omega_{pi}^2}{c^2} \right) \right\}^{1/2} \right] , \tag{4}$$

where $V_A = (B^2/4\pi n m_i)^{1/2}$, $\omega_{pi} = 4\pi n e^2/m_i$, $L_n = (\partial \ln n/\partial y)^{-1}$, $\beta = 2C_s^2/\gamma_s V_A^2$, and $C_s^2 = \gamma_s T/m_i$. The Hall term leads to a new drift mode in the limit $L_n < (c/\omega_{pi}) \times (1+\beta/2)^{-1/2}$. For $L_n \ll (c/\omega_{pi})(1+\beta/2)^{-1/2}$ the dispersion relation is $\omega \simeq k_x V_A (c/\omega_{pi})/L_n$ and the wave propagates in the $\mathbf{B} \times \nabla n$ direction.

The 2D Hall MHD code used in the analysis is based upon a finite volume method utilizing a variation of the beam scheme [17,18]. Equations (1)-(3) are solved in conservative form using a total variation decreasing scheme [19]. A nonlinear switch between an eighth-order spatial scheme and a low-order scheme based upon the partial donor cell method [20] is used. The temporal scheme is accurate to second order. The code has successfully modeled the nonlinear evolution of the unmagnetized ion Rayleigh-Taylor instability [21], sub-Alfvénic plasma expansions [22], and high-frequency magnetic drift waves [16]; all of these phenomena depend critically upon the Hall term. Simulations of the Kelvin-Helmholtz instability based upon ideal and Hall MHD were performed to benchmark the code. For example, from Fig. 7 of Fujimoto and Terasawa [15] one finds that $\gamma L/V_A \simeq 0.08$ for $k_x L = 0.4$; a simulation using these parameters yields a growth rate $\gamma L/V_A \simeq 0.08$ in agreement with theory. Opp and Hassam [14] obtained analytical results based upon idealized plasma and field profiles. Simulations were performed using parameters specified in Fig. 4 of their paper. The theoretical growth rate is $\gamma \simeq 0.21 V_0/L$ for $kL \simeq 0.52$; the growth rate obtained numerically is $\gamma \simeq 0.18 V_0/L$. The slightly lower numerical growth rate is attributed to approximate plasma and field profiles.

The simulations consider the plasma and field dynamics transverse to the ambient magnetic field. The plasma

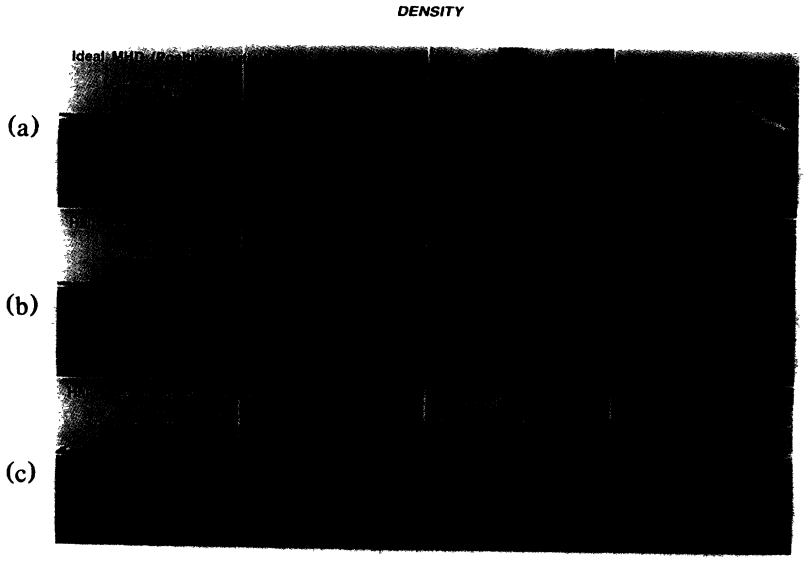

FIG. 1. Grey-scale contour plots of the density are shown at times $\Omega_{ic}t=1.76$, 6.16, 10.6, and 15.0 (i.e., $t\simeq 2$, 7, 12, and 17 sec) for three cases: (a) ideal MHD with positive vorticity, (b) Hall MHD with positive vorticity, and (c) Hall MHD with negative vorticity.

and field configurations used in the simulations are the following. The initial density, magnetic field, and velocity profiles are $n(y)=(n_0/2)[1+\Delta n-(1-\Delta n)\tanh(y/L_y)]$, $V(y)=V_0\tanh(y/L_y)\mathbf{e}_x$, and $B(y)$ satisfies pressure balance (i.e., $P+B^2/8\pi=\text{const}$). The parameters used are $n_0=10\ \text{cm}^{-3}$, $\Delta n=10$, $B(y=y_t)=1$ nT (y_t is the position of the top boundary), $C_s=3.0\times10^6$ cm/sec, $V_0=-6.8\times10^6$ cm/sec, and $L_y=5\times10^5$ cm. The simulation box extends from $x=0$ to 1.2×10^7 cm in the x direction, and from -2.1×10^7 to 2.1×10^7 cm in the y direction. The mesh size is $(x,y)=(80,100)$; the mesh is uniform in the x direction so that $\Delta x=1.5\times10^5$ cm, but is stretched in the y direction. The grid in the y direction is uniform between -3×10^6 and 3×10^6 cm for 60 cells so that $\Delta y=10^5$ cm; the remaining cells in the y direction are stretched. The boundary conditions are periodic in the x direction and are zero gradient (i.e., $\partial/\partial y=0$) in the y direction. The simulations are initialized with a 2% random perturbation in the fluid variables.

The parameters can be normalized to the density and magnetic field values at the center of the boundary layer, denoted by the subscript c (i.e., $n_c=55\ \text{cm}^{-3}$ and $B_c=9.22$ nT at $y=0$). The physical parameters at $y=0$ are $c/\omega_{pic}=3.1\times10^6$ cm, $\Omega_{ic}=0.88$ rad/sec, $\beta_c=1.2$, and $V_{Ac}=2.7\times10^6$ cm/sec. The key dimensionless parameters are $L/(c/\omega_{pic})=0.16$ and $V_0/V_A=2.52$. The phase velocity of the drift mode described by (4) is a maximum at $y\simeq-6\times10^5$ cm with a value $V_{ph}\simeq5.6\times10^7$ cm/sec

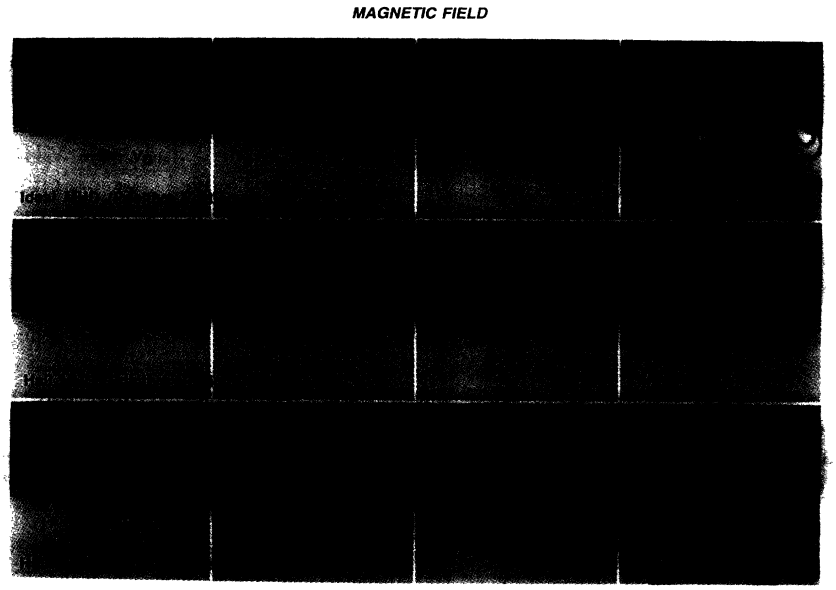

FIG. 2. Grey-scale contour plots of the magnetic field. The parameters and conditions are the same as in Fig. 1.

($\gg V_A$ and V_0). The dimensionless parameters are similar to those used by Thomas and Winske [8] in their study of the Venus ionopause, but in this Letter a narrower boundary layer is assumed initially, as well as cold ions.

The results of the simulation study of the Kelvin-Helmholtz instability are shown in Figs. 1 and 2. Grey-scale contour plots of the density (Fig. 1) and magnetic field (Fig. 2) are shown at times $\Omega_{ic}t = 1.8$, 6.2, 10.6, and 15.0 for three cases: (a) ideal MHD with positive vorticity ($\nabla\times\mathbf{V} > 0$), (b) Hall MHD with positive vorticity ($\nabla\times\mathbf{V} > 0$), and (c) Hall MHD with negative vorticity ($\nabla\times\mathbf{V} < 0$). These times correspond to $t \simeq 2$, 7, 12, and 17 sec. The size of each region shown is $x = 0$ to 2.4×10^7 cm (the actual simulation region is half this size) and $y = -10^7$ to 10^7 cm (the actual simulation region is roughly twice this size); this corresponds to $x/(c/\omega_{pic}) = 0$ to 7.7 and $y/(c/\omega_{pic}) = -3.2$ to 3.2. The total mass, magnetic flux, and vorticity are conserved to within a factor $\sim 5\times10^{-4}$ during the simulations. In Fig. 1 the most intense white region corresponds to a density $n > 150$ cm^{-3} and the darkest grey region to a density $n \sim 10$ cm^{-3}. In Fig. 2 the most intense white region corresponds to a magnetic field $B > 15$ nT and the darkest grey region to a magnetic field $B \sim 1$ nT.

The ideal MHD case is dominated by a single wave mode with a wavelength in $\lambda_x = 1.2\times10^7$ cm ($k_xL \simeq 0.26$), and a linear growth rate $\gamma = 0.49$ sec^{-1} ($\simeq 0.04V_0/L$); this result is consistent with linear theory (see Fig. 3 of Miura and Pritchett [23]). The largest density perturbations extend into the high density region ($y > 0$), and the largest magnetic field perturbations extend into the high field region ($y < 0$). The maximum velocity in the y direction occurs for $t \geq 15$ sec and is $|V_y| \simeq 4.0\times10^6$ cm/sec $\leq V_0$; this corresponds to vortex formation and the plasma "rolling up." Simulations were performed for the negative vorticity ideal MHD case; the results are the "mirror image" of the positive vorticity ideal MHD case.

The Hall MHD simulations are also dominated by a single wave mode. The linear growth rate for both Hall cases is roughly $\gamma \sim 0.04V_0/L$, which is the same as the ideal MHD case; this is in agreement with the linear theory of Fujimoto and Terasawa [15] who report little affect of Hall dynamics on the linear growth rate of the Kelvin-Helmholtz instability for $kL \leq 0.4$. However, the Hall MHD cases develop enhanced levels of small-scale turbulence ($kL \geq 1$); this result is also consistent with expectations from linear theory [14]. The small-scale turbulence saturates at low amplitudes and eventually the longest wavelength mode dominates in the evolution of the instability. Furthermore, the maximum velocity in the y direction is $|V_y| \simeq 2.0\times10^6$ cm/sec for the negative vorticity case, and $|V_y| \simeq 1.4\times10^6$ cm/sec for the positive vorticity case; these velocities are smaller than those for the ideal MHD case. Thus, the Hall term acts to inhibit vortex formation, as well as to relax sharp density and magnetic field structures as shown in Figs. 1 and 2. There is also a marked difference in the evolution of the density and magnetic field fluctuations in Hall MHD for positive and negative vorticity. The positive and negative vorticity cases are not mirror images of one another, as is the case for ideal MHD. The asymmetry is caused by the magnetic drift mode [16,24] which propagates in the $\mathbf{B}\times\nabla n$ direction. The asymmetry can develop because $\mathbf{V}\cdot\mathbf{V}_{ph}$ changes sign throughout the boundary layer for different signs of the vorticity.

The average density and magnetic field profiles in the y direction at times $\Omega_{ic}t = 0$ and 17.6 ($t = 0$ and 20 sec) are shown in Fig. 3. The average profile is defined as $\langle n(y), B(y)\rangle = \int[n(x,y), B(x,y)]dx/\int dx$ and the limits of integration extend from $x = 0$ to 1.2×10^7 cm, the size

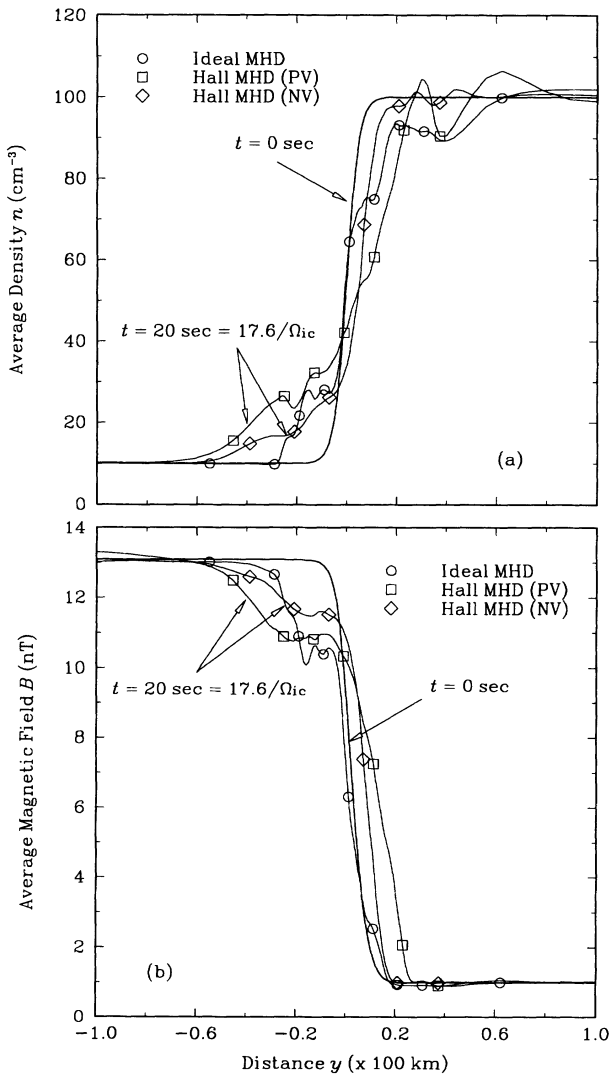

FIG. 3. Average profiles of (a) density and (b) magnetic field at times $\Omega_{ic}t = 0$ and 15.0 (i.e., $t \simeq 0$ and 20 sec) for the three cases studied (see Fig. 1). Here, PV denotes positive vorticity and NV negative vorticity.

of the simulation box. The positive vorticity Hall MHD case leads to the most rapid broadening of the boundary layer; the density boundary layer thickness grows from $L\sim 5$ km to $L\sim 140$ km. This is in contrast to the ideal MHD and negative vorticity Hall MHD case in which the density boundary layer thickness grows from $L\sim 5$ km to $L\sim 90$ km. The magnetic field boundary layer also increases its width in all cases. The most significant difference between the ideal MHD case and the Hall MHD cases is the enhanced diffusion of the magnetic field into the high density, low magnetic field region (i.e., $y>0$) for the Hall MHD cases. This is caused by magnetic field transport via magnetic drift waves associated with the density irregularities in the region $y>0$ [16,24].

Thus, the nonlinear evolution of the Kelvin-Helmholtz instability in narrow boundary layers ($L<c/\omega_{pi}$) is dramatically altered by the Hall term. Short wavelength turbulence is generated ($kL>1$) which inhibits vortex formation, and there is an asymmetry associated with the direction of the vorticity. This suggests that boundary layer turbulence associated with a magnetized plasma flowing past an unmagnetized body (such as Venus or a cometary ionopause) or a magnetized body (e.g., the Earth's magnetopause) may be asymmetric in the east-west direction (where the interplanetary magnetic field is in the north-south direction). Interestingly, hybrid simulations of a "cometlike" obstacle in the solar wind observe such an anisotropy [25]. There are also potential applications to laboratory plasmas. For example, the laser-target experiments of sub-Alfvénic plasma expansions [5] are dominated by Hall MHD physics, especially in the early time structuring of the plasma and field. Following the formation of "plasma jets," secondary structures formed on the sides of the jets which may be due to the Kelvin-Helmholtz instability.

Finally, several other points are worth noting. First, finite Larmor radius effects, associated with an anisotropic ion stress tensor [26], are expected to be important in the regime $L\sim\rho_i$. As a point of reference, $\rho_i\sim c/\omega_{pi}$ for $\beta_i\simeq 1$. This effect has a stabilizing influence on the Kelvin-Helmholtz instability [27]. The code is being upgraded to incorporate this effect. Second, the assumption of an isothermal plasma can break down; simulations using an adiabatic equation of state will be reported elsewhere. And third, the plasma and field configuration should be extended to allow for dynamics parallel to the ambient magnetic field; for this situation the Hall term leads to whistler waves [13].

We thank Dr. Peter Cargill for several helpful discussions and a critical reading of the manuscript, and Dr. John Lyon, Dr. Clark Mobarry, and Dr. Steve Zalesak for discussions regarding numerical techniques. This research has been supported by the Office of Naval Research, and the National Aeronautics and Space Administration under the Venus Data Analysis Program.

[1] N. Sckopke, G. Paschmann, G. Haerendel, B. U. O. Sonnerup, S. J. Bame, T. B. Forbes, E. W. Hones, Jr., and C. T. Russell, J. Geophys. Res. **86**, 2099 (1981).
[2] J. Berchem and C. T. Russell, J. Geophys. Res. **87**, 2108 (1982).
[3] F. M. Neubauer, J. Geophys. Res. **93**, 7272 (1988).
[4] J. G. Luhmann and T. E. Cravens, Space Sci. Rev. **55**, 201 (1991).
[5] B. H. Ripin, E. A. McLean, C. K. Manka, C. Pawley, J. A. Stamper, T. A. Peyser, A. N. Mostovych, J. Grun, A. B. Hassam, and J. D. Huba, Phys. Rev. Lett. **59**, 2299 (1987).
[6] J. D. Huba, J. Geophys. Res. **86**, 8991 (1981); G. Ganguli, Y. C. Lee, and P. J. Palmadesso, Phys. Fluids **31**, 821 (1988); Z. Wang, P. L. Pritchett, and M. Ashour-Abdalla, Phys. Fluids B **4**, 1092 (1992).
[7] P. J. Cargill and T. E. Eastman, J. Geophys. Res. **96**, 13763 (1991).
[8] V. A. Thomas and D. Winske, Geophys. Res. Lett. **18**, 1943 (1991); J. Geophys. Res. **98**, 11425 (1993).
[9] T. Terasawa, M. Fujimoto, H. Karimabadi, and N. Omidi, Phys. Rev. Lett. **68**, 2778 (1992).
[10] J. Berchem and H. Okuda, J. Geophys. Res. **95**, 8133 (1990).
[11] S. Chandrasekhar, *Hydrodynamic and Hydromagnetic Stability* (Dover, New York, 1961).
[12] A. Miura, J. Geophys. Res. **92**, 3195 (1987).
[13] A. B. Hassam and J. D. Huba, Phys. Fluids **31**, 318 (1988).
[14] E. Opp and A. B. Hassam, Phys. Fluids B **3**, 885 (1991); E. Opp, Ph.D. thesis, Maryland, 1992.
[15] M. Fujimoto and T. Terasawa, J. Geophys. Res. **96**, 15725 (1991).
[16] J. D. Huba, Phys. Fluids B **3**, 3217 (1991).
[17] R. H. Sanders and K. H. Prendergast, Astrophys. J. **188**, 489 (1974).
[18] J. G. Lyon (private communication).
[19] A. Harten, J. Comput. Phys. **49**, 357 (1983).
[20] K. H. Hain, J. Comput. Phys. **73**, 131 (1987).
[21] J. D. Huba, J. G. Lyon, and A. B. Hassam, Phys. Rev. Lett. **59**, 2971 (1987).
[22] J. D. Huba, P. A. Bernhardt, and J. G. Lyon, J. Geophys. Res. **97**, 11 (1992).
[23] A. Miura and P. L. Pritchett, J. Geophys. Res. **87**, 7431 (1982).
[24] A. S. Kingsep, K. V. Chukbar, and V. V. Yan'kov, in *Reviews of Plasma Physics*, edited by B. B. Kadomtsev (Consultants Bureau, New York, 1990), Vol. 16.
[25] V. A. Thomas and D. Winske (private communication).
[26] K. V. Roberts and J. B. Taylor, Phys. Rev. Lett. **B**, 197 (1962).
[27] D. L. Jassby, Phys. Fluids **15**, 1590 (1972).

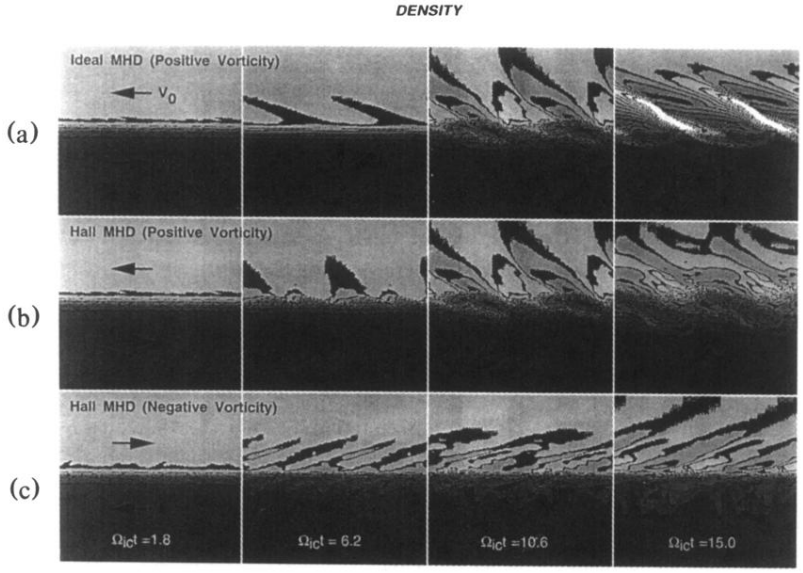

FIG. 1. Grey-scale contour plots of the density are shown at times $\Omega_{ic}t = 1.76$, 6.16, 10.6, and 15.0 (i.e., $t \simeq 2$, 7, 12, and 17 sec) for three cases: (a) ideal MHD with positive vorticity, (b) Hall MHD with positive vorticity, and (c) Hall MHD with negative vorticity.

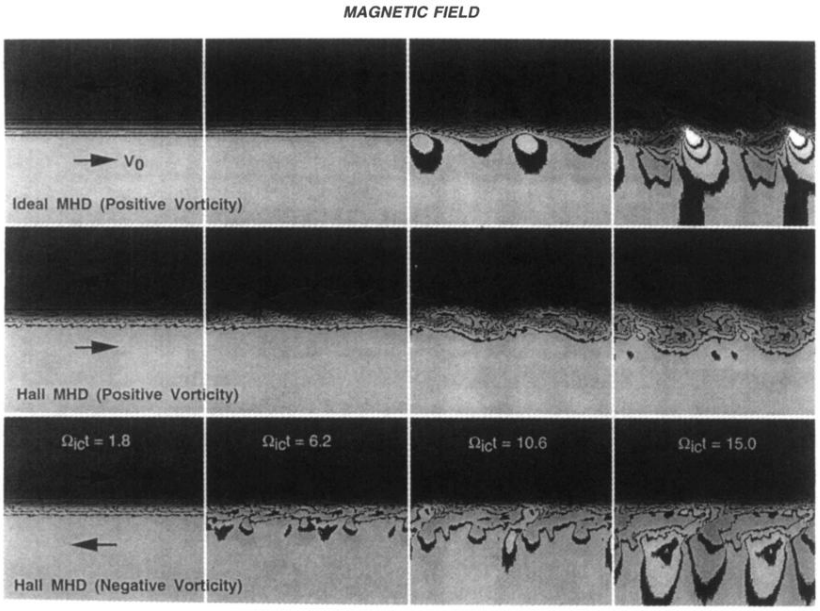

FIG. 2. Grey-scale contour plots of the magnetic field. The parameters and conditions are the same as in Fig. 1.